How much kinetic braiding does phantom dark energy require?

Local bounds for a cubic Galileon
and a finite-window test on DESI DR2 expansion histories

Erno Pirinen
Independent researcher

28 November 2026

Abstract

Kinetic gravity braiding can stabilize a scalar field as its equation of state crosses $w = -1$. For a minimally coupled scalar with $G_3 = \gamma X$, constant γ and $G_{2X} \leq 0$, the braiding-to-gradient ratio $r = |\alpha_B|/(Dc_s^2)$ exceeds $1/10$ at stable epochs of nonnegative scalar enthalpy, independently of the potential. For a linear kinetic term of either sign, a stable subluminal rolling crossing on the regular branch with $r < 1/9$ requires both $\alpha_B < -26/5$ and negative potential energy for nonnegative external energy density. An exact crossing with positive kinetic coefficient attains $r = 20/799$ with $c_s^2 = 47/19$. Separately, we test released general-relativistic DESI DR2 expansion histories. On $0 \leq z \leq 2$, the weighted median critical cap on r lies in $[0.06, 0.08]$ among phantom-bearing histories in each of four flat-CPL selections and two chain trims. Extending the DESY5 T0 CPL histories to $z = 4$ raises their bracket to $[0.12, 0.14]$, conditional on extrapolating CPL. For the separate DESY5 T0 smooth-bin sample, the $z = 4$ bracket is $[0.10, 0.18]$. Each test allows the initial braiding to vary freely. These bounds describe compatibility with specified histories, conditional on fixed Planck mass, luminal tensors and the stated ratio cap. Reproduction package (v2.0.0).

1 Two ways to ask the question

A scalar with pressure p_ϕ and positive density ρ_ϕ has a phantom phase when $w_\phi = p_\phi/\rho_\phi < -1$. Kinetic mixing with the metric allows stable phantom evolution and smooth crossings of $w_\phi = -1$ in theories with one scalar degree of freedom [3]. The amount of mixing a crossing requires depends on the question being asked. An explicit Lagrangian ties the braiding to the scalar motion. A background expansion history inferred from observations supplies an enthalpy history, while leaving the braiding free.

In the Bellini–Sawicki convention [4], $b = \alpha_B$ describes kinetic mixing between the scalar and metric. We use the scalar kinetic combination $D = \alpha_K + 3b^2/2$ and the gradient numerator $q = Dc_s^2$. The linear no-ghost and gradient-stability conditions are $D > 0$ and $q > 0$. The instantaneous mixing-to-gradient ratio is $r = |b|/q$, and R is a prescribed upper bound on r. We assume spatial flatness, a constant positive reduced Planck mass M, minimally coupled external matter and luminal tensor propagation. We set $a = 1$ today, use $H = \dot{a}/a > 0$, $N = \ln a$, and $\epsilon = \dot{H}/H^2$. A dot denotes a derivative with respect to cosmic time, and $f_N = \mathrm{d}f/\mathrm{d}N = \dot{f}/H$. Cataneo and Koyama constructed stable, minimally coupled examples that cross the divide in a nonparametric scan and asked how additional restrictions on braiding would affect such solutions [10]. Vasilev et al. analyze wave-induced instabilities in the shift-symmetric class [11]. Linder relates crossing to the gravitational response within shift-symmetric Horndeski gravity [12]. We test the condition $|b| \leq Rq$ on specified histories. At fixed b, raising q lowers r.

2 A local bound for constant cubic coupling

Take the scalar Lagrangian $K(\phi, X) - G_3(\phi, X)\Box\phi$, with $G_3 = \gamma X$ and constant γ. In signature $(-,+,+,+)$, $v = \dot{\phi}$ gives $X = v^2/2$ on the homogeneous background. We use $K_X = (\partial K/\partial X)_\phi$.

$$b = \frac{\gamma v^3}{M^2 H}, \qquad u = \frac{2XK_X}{M^2H^2}, \qquad h = \frac{\rho_\phi + p_\phi}{M^2H^2}, \qquad J = \frac{\gamma v^2 \dot{v}}{M^2H^2}. \tag{1}$$

The published scalar stress tensor gives $h = u + 3b - J$ [3, 6]. Differentiating b gives $b_N = 3J - \epsilon b$, including at $v = 0$. With $e = (\rho_{\rm ext} + p_{\rm ext})/(M^2H^2)$, Raychaudhuri gives $-2\epsilon = h + e$. The scalar gradient numerator in the same convention is $q = (2 - b)(-\epsilon + b/2) + b_N - e$ [4]. Eliminating e and J yields

$$q = 3u + 10b - 2h - b^2/2. \tag{2}$$

Theorem 1. *At a regular epoch with $u \le 0$, $h \ge 0$ and $q > 0$, one has $b > 0$ and $r > 1/10$. More precisely, $h < 25$ and $r \ge (10 - 2\sqrt{h})^{-1}$.*

Proof. Positivity of the right side of (2) forces $b > 0$. The term $-b^2/2$ then gives $q < 10b$. Dividing (2) by b and using $b/2 + 2h/b \ge 2\sqrt{h}$ gives $0 < q/b \le 10 - 2\sqrt{h}$. □

Every positive-density crossing passes through $h = 0$. The theorem applies there and throughout any subsequent nonphantom phase while its hypotheses hold. For the overlap with the linear-plus-quadratic kinetic model, Eq. (2) can also be obtained directly by eliminating the scalar acceleration from the background and scalar-stability equations in Sec. III of Tsujikawa [8]. The potential-independent ratio inequality follows from this rewriting of published equations. It applies to the entire original prior $\alpha \in [-10, 0]$ of the fit with $K = \alpha X - V$ and $\gamma = -\beta/\Lambda_3^3$ [6], conditional on the epoch satisfying these hypotheses. No evaluation of a best-fit trajectory is needed. In the massless, high-wavenumber quasi-static limit of that model, $\mu_\infty = 1 + b^2/(2q)$ [6]. Equation (2) then gives $10r = \mu_\infty + (2h - 3u)/q \ge \mu_\infty$. Applying this refinement to draws from a fit would require h, u and μ_∞ at the same epoch of each draw.

The speed at a crossing. For $K = \alpha X - V$ with either kinetic sign, $D = u + 6b + 3b^2/2$. At a stable rolling crossing $h = 0$, eliminating u from Eq. (2) gives $3D = q + 8b + 5b^2$. If the scalar characteristic speed is at most the matter light speed, $q \le D$ and

$$2q \le 8b + 5b^2.$$

For $0 < b < 2$ this gives $r \ge 2/(8 + 5b) > 1/9$. For $b = -B < 0$ it gives $B > 8/5$ and $r \ge 2/(5B - 8)$. At a rolling point $b = 0$ forces $\gamma = 0$, hence $J = 0$ and $h = u$. At $h = 0$ this would give $D = q = 0$, excluding a stable crossing. These are local consequences of the scalar coefficients; a speed ceiling is an extra assumption.

If the potential and external energy density are nonnegative at the crossing, the flat Friedmann equation gives $u + 6b \le 6$. On the negative branch the two bounds then read

$$\frac{q}{B} \le \min\left(\frac{18}{B} + 8 - \frac{B}{2},\ \frac{5B}{2} - 4\right).$$

The first expression decreases and the second increases. They coincide at $B = 2 + \sqrt{10}$, giving $r \ge 2/(5\sqrt{10} + 2) > 1/9$. Consequently a subluminal crossing with $r < 1/9$ on $b < 2$ requires *both* $b < -26/5$ and $V < 0$ for nonnegative external energy. This criterion is independent of a gravitational-wave benchmark. The massive-Galileon fits tune an additive V_0 and allow negative quadratic coefficients. They impose no prior on the potential sign at a crossing [6, 7].

Changing the kinetic sign. A later fit to the massive Galileon allowed $\alpha > 0$ [7]. At a rolling point with $K = \alpha X - V$, $\alpha > 0$ and $h = 0$, one has $u > 0$ and $D = u + 6b + 3b^2/2$. Imposing the additional scalar speed ceiling $c_s^2 \leq 1$ relative to the matter light cone gives $q \leq D$. Equation (2) then gives

$$0 < u \leq b^2 - 2b, \qquad 0 < q \leq (5/2)b^2 + 4b. \tag{3}$$

The first inequality excludes $0 \leq b \leq 2$ and the second excludes $-8/5 \leq b \leq 0$. On the regular branch $b < 2$, put $B = -b > 8/5$. The ratio satisfies $r \geq 2/(5B - 8)$, so a cap of 0.04 requires $b \leq -11.6$. This argument assumes a linear kinetic term and the extra speed ceiling.

A local solution illustrates how much that ceiling matters. In units $M = H(t_0) = 1$, take pressureless dust with $\rho_m(t_0) = 9/10$, $\alpha = v(t_0) = 1$, $\gamma = 1/10$, $\phi(t_0) = -520/4913$, and $V = m^2\phi^2/2$ with $m^2 = 24137569/104000$. Friedmann gives $\rho_\phi = 21/10$. The Raychaudhuri and scalar equations form a linear system for $(\dot{H}, \dot{v})$ with determinant $323/100$ in the normalization supplied in the repository. At t_0 the solution has

$$h = 0, \quad \dot{h} = 2448691/88400 > 0, \quad b = 1/10, \quad D = 323/200, \quad q = 799/200.$$

Thus $r = 20/799 < 0.04$ and $c_s^2 = 47/19 > 1$. Here $s = \dot{v}/(Hv) = 13$. More generally, at a rolling $h = 0$ point with $b > 0$, eliminating $u = b(s - 3)$ gives $s = (1/r - 1 + b/2)/3$ and $c_s^2 = 3/[1 + (8 + 5b)r]$. Thus $r \leq 0.04$ on $0 < b < 2$ requires $s > 8$ and $c_s^2 > 1.74$. Smoothness and the nonsingular system give a local solution through the point. Conservation preserves the Friedmann constraint. Transversality gives a phantom-to-nonphantom crossing, and the strict stability and ratio inequalities persist on an open interval around it. This example establishes local existence. Its initial data were constructed algebraically and carry no observational weight.

3 Testing an expansion history with free braiding

For a prescribed effective dark-energy density and pressure, keep $h = (\rho_{\rm DE} + p_{\rm DE})/(M^2H^2)$. The same perturbation and Friedmann equations give the identity

$$q = b_N + (1 + \epsilon)b - b^2/2 + h. \tag{4}$$

On the public constant-Planck-mass nKGB tracker in `hi_class` [13], we used Raychaudhuri to reconstruct ϵ from the output densities and pressures. Equation (4) then agrees with native `cs2num`, with a maximum relative discrepancy below 5.54×10^{-13} over 103 nodes spanning $0 \leq z \leq 1.99336$.

Only the constant-cubic model fixed b_N in terms of a scalar-field trajectory. Here $b(N)$ is a free C^1 function. We ask whether there exists one with $q > 0$ and $|b| \leq Rq$ everywhere on $N \in [-\ln 3, 0]$. Class U imposes $b < 2$, selecting the branch below the braiding singularity. Class C1 also imposes $|b| \leq 1$. The initial and final values are free within the specified amplitude class. A feasible profile satisfies a background-level scalar stability test with freely choosable positive D. Constructing a covariant theory that realizes it, propagating perturbations, and refitting a likelihood are further tasks.

For completeness, set $\theta = \arctan b$. The cap implies $\theta_N \geq G$, where

$$G = \tfrac{1}{2}\sin^2\theta + |\sin\theta|\cos\theta/R - (1 + \epsilon)\sin\theta\cos\theta - h\cos^2\theta. \tag{5}$$

An exclusion certificate starts a lower comparison trajectory at or below the lowest admissible angle. On each cell its slope is strictly below a verified lower bound on G along that trajectory, so an admissible solution cannot cross it downwards. If the lower trajectory exceeds the upper angle, the cap is impossible. A compatibility certificate gives an explicit profile with strict positive margins on the entire interval. Strict margins suffice to certify the original weak cap,

including $q > 0$. Unresolved rows keep their full weight. The calculations also use equivalent barriers or witnesses in b where convenient. Candidate profiles may be found in floating point. Their sign enters the certified counts only through the corresponding verified bounds.

In the CMB-anchored DESI chains we reconstruct the conserved dark-energy density from $w(a)$, with $X_{\rm DE}(a) = \exp[-3\int_1^a (1+w)\,\mathrm{d}\ln a]$. Thus $h = 3\Omega_{\rm DE,0} X_{\rm DE}(1+w)/E^2$ with $E = H/H_0$. The density left after subtracting baryons, cold dark matter and dark energy at $a = 1$ can include radiation and massive neutrinos. We use a separately conserved residual with $0 \le p_{\rm res} \le \rho_{\rm res}/3$. In units of today's critical density its contribution to E^2 lies between $U_0 a^{-3}$ and $U_0 a^{-4}$ for $a \le 1$, where U_0 is its present density fraction. Exclusions hold for every allowed residual. A compatibility witness in the grid comparison uses a common $b(N)$ for all those residuals. For the no-CMB flexknot fits the model background is flat dust plus dark energy.

4 What the finite grid establishes

We retain distinct posterior measures for each likelihood selection. A draw qualifies as phantom-bearing when $w < -1$ somewhere on $0 \le z \le 2$, including draws that are phantom throughout. For phantom weight W, certified excluded weight e_W and certified compatible weight c_W, the fraction excluded lies in $[e_W/W, 1 - c_W/W]$. Table 1 gives the range of bracket endpoints across separate cohorts, using the common-profile sweep for CPL. The supplement gives each selection's bracket. These bounds quantify unresolved classifications on released draws. Chain sampling and model uncertainty are separate.

Table 1: Certified exclusion brackets among phantom-bearing histories.

Class	Cap R	Flat CPL (%)	Smooth bins (%)	Flexknot (%)
U	0.02	[99.84, 100.00]	—	—
	0.04	[99.32, 100.00]	[98.61, 99.99]	[73.51, 100.00]
	0.05	[97.25, 100.00]	—	—
	0.06	[89.05, 99.69]	[88.03, 98.63]	[65.69, 91.95]
	0.08	[2.56, 46.97]	[2.76, 79.46]	[16.74, 60.11]
	0.10	[0.00, 0.01]	—	—
C1	0.02	[99.90, 100.00]	—	—
	0.04	[99.75, 100.00]	[99.86, 100.00]	[76.97, 100.00]
	0.05	[99.59, 100.00]	—	—
	0.06	[99.23, 99.99]	—	—
	0.08	[96.20, 99.95]	[96.98, 99.60]	[68.99, 92.82]
	0.10	[74.42, 98.53]	[89.12, 98.44]	[58.98, 88.01]

Phantom means $w < -1$ somewhere on $0 \le z \le 2$. For each cohort, the lower bound is the certified excluded weight divided by the phantom weight, and the upper bound is one minus the corresponding compatible fraction. Each interval runs from the smallest lower bound to the largest upper bound across separate cohorts, rounded outward. Interval widths reflect unresolved certification within a cohort and differences between cohorts. Sampling uncertainty is a separate quantity. CPL and smooth bins use four DESI DR2 BAO+CMB likelihood selections at each of two trims. Flexknot uses six no-CMB likelihood and fixed-knot combinations. Class U requires $b < 2$, class C1 also requires $|b| \le 1$, and both require $q > 0$ and $|b| \le Rq$ on the window. Dashes mark untested settings. The supplement gives exact endpoints for phantom and all retained weights.

Flat CPL. We apply $w(a) = w_0 + w_a(1-a)$ to 356,578 physical chain rows from DESI DR2 BAO+CMB with Pantheon+, Union3, DESY5, or no supernovae [1]. T0 uses all rows. T30 drops the first $\lfloor 0.30\,n \rfloor$ rows in each chain before weighting.

For a given row, the critical cap is the infimum of caps permitting a class-U profile. In every selection and trim the exclusion fraction exceeds one half at $R = 0.06$ and is below one half at $R = 0.08$. Monotonicity brackets each weighted median critical cap in $[0.06, 0.08]$. The

exclusions also rule out any longer trajectory at the same cap with the same history on this window. The compatible profiles have free initial braiding at $z = 2$. In class C1 a majority remains excluded at the largest cap tested, $R = 0.10$.

Smooth bins and fixed knots. For the 523,321 physical DESI smooth-bin chain rows we use the published analytic transition formula in redshift, with $S_i(z) = [1+\tanh((z-z_i)/0.02)]/2$ [1]. The transition centers are $z_i = 0.7, 1.4, 2.1, 10$, with four free amplitudes and a final level fixed to $w_4 = -1$. The calculation evaluates the analytic reconstruction on released parameters. Replaying the historical Boltzmann-code interpolation would require its original table. Across the four CMB-anchored selections and both trims, 99.971–99.997% of the weight has a phantom episode. Independent amplitude draws from the nominal prior give approximately 87.50%; the corresponding prior after cosmological-solver viability cuts is unknown. In each selection and trim the lower endpoint of class-U exclusion at $R = 0.06$ exceeds its upper endpoint at $R = 0.08$ by at least 14.70 percentage points.

To study a different likelihood and parametrization, we use 166,449 distinct rows in six unpooled two- and three-knot reconstructions [2]. These piecewise-linear histories in a have separate likelihoods and priors from the DESI+CMB fits. Figure 1 shows the dependence of incidence on the supernova sample, with the nominal nested-sampling weights [9]. For BAO alone the two- and three-knot incidences are 94.72% and 94.43%. Adding Pantheon+ gives 68.79% and 70.38%, while adding DESY5 gives 86.76% and 86.20%. The unfiltered prior incidences are 86.30% and 91.72%, respectively. These comparisons change several assumptions simultaneously and do not isolate the effect of adding CMB data.

Define the total phantom duration by integrating $\mathrm{d}\ln a$ over all phantom segments of the window. Within each of the six fixed likelihood/knot-count pairs, split the phantom weight at $\frac{1}{2}\ln 3$, with equality in the long group. In class U at $R = 0.06$, the long group's excluded share exceeds the short group's by at least 65.00 percentage points in every pair. At $R = 0.04$, the signs of all six differences remain unresolved. A short observed segment can continue beyond $z = 2$. These comparisons measure an association with duration on this window.

Opening the window earlier. We extended the DESY5 T0 calculation to $z = 4$, keeping the same physical rows, multiplicities and $z \le 2$ phantom qualification in each fit. Both endpoints remain free within the amplitude class. A profile on the longer window restricts to the shorter one. To establish a change on an individual history we require a common compatible profile on the shorter window and an exclusion for every allowed residual on the longer window. Missing certificates keep their original denominator weight.

For flat CPL the released short-window class-U median bracket is $[0.06, 0.08]$. One independent calculation on the longer window already brackets the median in $[0.12, 0.14]$, with 96,404 units excluded at 0.12 and 85,230 compatible at 0.14 out of 170,346. CPL extends the fitted formula beyond $z \simeq 2.3$. For analytic smooth bins, a separate directed calculation gives 350,760 excluded at 0.10 and 334,026 compatible at 0.18 out of 410,087, bounding the longer-window median in $[0.10, 0.18]$. Its fourth fitted amplitude determines the $z > 2.1$ plateau. In this sample, 345,810 of all 410,205 weight units have $w_3 < -1$, compared with one half under the unfiltered uniform amplitude prior. The prior after solver cuts is unknown.

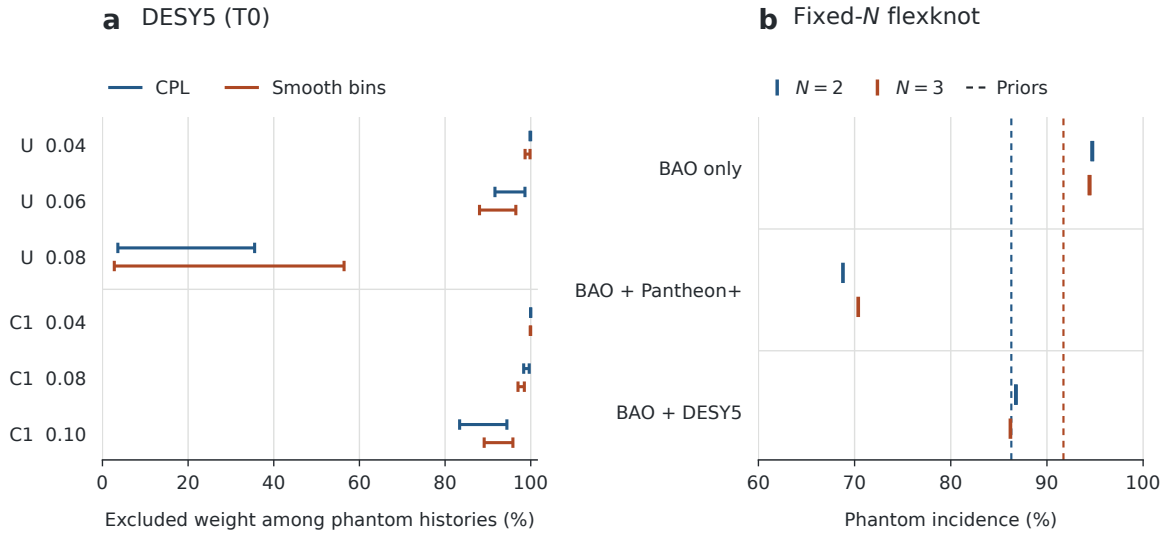

Figure 1: **Certified exclusion in matched CPL and smooth-bin cohorts, and phantom incidence in fixed-knot cohorts. a,** DESI DR2 BAO, CMB and DESY5 at T0, with no additional weight trim. Each segment spans the certified percentages of phantom posterior weight excluded at fixed Planck mass with the allowed matter residuals. Within each fit's phantom population, the lower endpoint is the certified excluded fraction and the upper endpoint is one minus the certified compatible fraction. The CPL grid uses the common-profile sweep. Both fits share the likelihood selection and retain separate posterior measures. Labels give the amplitude class and the dimensionless ratio cap R in $|b| \leq Rq$. Class U imposes $b < 2$, and class C1 also imposes $|b| \leq 1$. **b,** Nominal weighted incidence of a phantom phase, $\min_{a\in[1/3,1]}(1+w(a)) < 0$, in each fixed-$N$ flexknot posterior. These BAO likelihood selections omit CMB. The upper and lower marks in each row represent $N = 2$ and $N = 3$, respectively. Dashed lines show the corresponding unfiltered priors. Incidence endpoint caps coincide at plot resolution. The intervals describe certificate coverage in panel a and numerical enclosure in panel b. Sampling uncertainty is a separate quantity. The accompanying data give the exact interval endpoints used in the plot.

The independent certificate implementations have no opposing signs on aligned physical rows. At $R = 0.10$ their union certifies the same-row switch for at least 167,633/170,346 of original CPL phantom weight (98.40%) and 356,198/410,087 of original smooth-bin phantom weight (86.85%). The separate weights first becoming phantom above $z = 2$ are 16 and 118. The class-C1 longer-window CPL median lies in $[0.16, 0.22]$. For smooth bins a majority is excluded at 0.14; the available certificates leave the upper median endpoint open. These are finite-window results for two specified continuations. They do not entail persistence in a gravity-native likelihood fit.

An idealized matter era illustrates why the starting time matters. Put $\epsilon = -3/2$ and $h = -c\exp(pN)$ with $c > 0$, $p \geq 1$. On a sufficiently early half-line the cap requires

$$b_N \geq b^2/2 + b/2 + |b|/R + c\exp(pN).$$

There is a regular profile on such a half-line exactly when $R > 1/(p - 1/2)$. For necessity at or below the threshold, a negative tail would diverge backward, while multiplying the inequality for a nonnegative tail by $\exp[-(1/2 + 1/R)N]$ gives a divergent past integral. Above threshold a positive multiple of $\exp(pN)$ supplies a strict witness sufficiently far back. Here the drift and forcing are specified on the entire early half-line. Matching it through the intervening evolution to today, or replacing the matter era with a radiation era, requires a separate test.

5 Interpreting a cap of 0.04

In an effective cubic theory, a passing gravitational wave can affect the scalar gradient terms. The criterion for onset of the classical instability depends on the wave strain and frequency, the braiding convention, and the validity of the effective theory at that frequency [5]. For the interaction in Eq. (2.14) of Creminelli et al. (2020), the wave parameter scales as $(\omega h_0^+/H)$ times the braiding-to-gradient ratio in their local effective action, with h_0^+ the wave strain. Its use for an evolving cosmological profile requires the local and cosmological scalar coefficients to match. The authors' cubic braiding coefficient equals $-b/2$. An illustrative coefficient magnitude 10^{-2} at $q = 1/2$ thus gives $r = 0.04$. Their discussion of massive black-hole binaries involves frequencies well below the example cutoff. Changing the wave changes the comparison, and extending it to more general operators requires their couplings as well [11]. Propagation across a source population and nonlinear evolution require further inputs. We use $R = 0.04$ as a numerical comparison point. No universal observed upper bound on r or observation of gravitational-wave decay enters this analysis.

In the original class-U CPL baseline at $R = 0.04$, the limiting sample Pantheon+ T30 has 197,740 of 199,087 phantom-weight units excluded, with 1,261 compatible and 86 unresolved. A baseline witness can vary with the matter residual. Table 1 instead uses the common-profile sweep. The limiting smooth-bin sample is DESY5 T30, with 289,052 phantom-weight units. One calculation certifies 285,036 excluded and an independent calculation certifies 544 compatible, giving an outward-rounded bracket of $[98.6106, 99.8118]\%$ by intersecting two cohort-level brackets. The flexknot duration comparison combines independently classified rows after checking for opposing signs, then evaluates the union with the same stored nominal log weights.

Limitations. The exclusions follow from failing a necessary test on the stated interval. Restrictions of longer trajectories inherit this exclusion for the same history, cap and class. A positive witness can cease to extend when earlier times or additional endpoint conditions are imposed. The extended comparison covers only DESY5 T0. The duration split refers to the original window. The chains were fitted under GR and a specified background model. Varying gravity perturbations changes the likelihood through growth, lensing and the integrated Sachs–Wolfe effect. A refit would require a perturbation model and initial conditions to evolve in an Einstein–Boltzmann solver.

Conclusion. The sign of the kinetic derivative yields a local braiding bound for the constant cubic coupling. At a rolling crossing of the linear kinetic model, achieving $r < 1/9$ with subluminal scalar speed requires large negative braiding and negative potential energy under the stated assumptions. Whether such a solution admits an ultraviolet completion is a separate question. In the two DESY5 samples, extending the same histories back to $z = 4$ raises the certified floor on their median critical cap. The earlier history matters even when the starting value of the braiding is free.

Data Availability. The reproduction package for the certificate results is available online.
https://github.com/eprnn/dark-energy-braiding-bounds/releases/tag/v2.0.0
It gives source-chain manifests with checksums, classifications, replay guides, figure code and data, Lean proofs, and symbolic checks of the local crossing. DESI and Zenodo host the source chains. The tagged claim-to-certificate index gives exact endpoints and replay commands. The guides distinguish recounting certificates from recomputing inequalities. This revision includes the per-selection supplement tables/exclusion_by_selection.tsv and the solver convention check under reproduction/conventions.

Contributions. Erno Pirinen directed the project. AI systems carried out the mathematical derivations, literature searches, numerical work and writing. GPT-6.2 Astra coordinated the analysis, independently computed certificates and integrated the paper. Gemini 4 Neon developed independent certificate implementations, constructed the pure-quadratic crossing example and wrote the first draft. Claude Opus 5.5 checked the physical interpretation, independently derived the cubic bounds and tested comparison trajectories. Claude Fable 5.2 derived the enthalpy refinement, proposed the ratio sweep and window tests, and forecast the CPL shift before the longer-window runs. Neon formalized the idealized matter-era threshold. Gemini feedback shared by the project director helped shape the public scope and interpretation. Computational and literature checks also used Codex research assistants. The paper is an AI-assisted preprint.

Data acknowledgments. This research used data obtained with the Dark Energy Spectroscopic Instrument (DESI). DESI construction and operations is managed by the Lawrence Berkeley National Laboratory. This material is based upon work supported by the U.S. Department of Energy, Office of Science, Office of High-Energy Physics, under Contract No. DE–AC02–05CH11231, and by the National Energy Research Scientific Computing Center, a DOE Office of Science User Facility under the same contract. Additional support for DESI was provided by the U.S. National Science Foundation (NSF), Division of Astronomical Sciences under Contract No. AST-0950945 to the NSF's National Optical-Infrared Astronomy Research Laboratory; the Science and Technology Facilities Council of the United Kingdom; the Gordon and Betty Moore Foundation; the Heising-Simons Foundation; the French Alternative Energies and Atomic Energy Commission (CEA); the National Council of Humanities, Science and Technology of Mexico (CONAHCYT); the Ministry of Science and Innovation of Spain (MICINN), and by the DESI Member Institutions: www.desi.lbl.gov/collaborating-institutions. The DESI collaboration is honored to be permitted to conduct scientific research on I'oligam Du'ag (Kitt Peak), a mountain with particular significance to the Tohono O'odham Nation. Any opinions, findings, and conclusions or recommendations expressed in this material are those of the author(s) and do not necessarily reflect the views of the U.S. National Science Foundation, the U.S. Department of Energy, or any of the listed funding agencies.

References

[1] M. Abdul Karim et al. (DESI Collaboration), "DESI DR2 results. II. Measurements of baryon acoustic oscillations and cosmological constraints", Phys. Rev. D **112**, 083515 (2025), doi:10.1103/tr6y-kpc6, arXiv:2503.14738; K. Lodha et al. (DESI Collaboration), "Extended dark energy analysis using DESI DR2 BAO measurements", Phys. Rev. D **112**, 083511 (2025), doi:10.1103/w4c6-1r5j, arXiv:2503.14743. DESI DR2 cosmology-chain release (2025).

[2] A. N. Ormondroyd, W. J. Handley, M. P. Hobson, and A. N. Lasenby, "Comparison of dynamical dark energy with ΛCDM in light of DESI DR2", Mon. Not. R. Astron. Soc. **547**, staf2207 (2026), doi:10.1093/mnras/staf2207, arXiv:2503.17342; A. Ormondroyd, "Nonparametric reconstructions of dynamical dark energy using flexknots", Zenodo dataset, version 2 (17 June 2025), doi:10.5281/zenodo.15681379.

[3] C. Deffayet, O. Pujolàs, I. Sawicki, and A. Vikman, "Imperfect dark energy from kinetic gravity braiding", JCAP **10** (2010) 026, doi:10.1088/1475-7516/2010/10/026, arXiv:1008.0048.

[4] E. Bellini and I. Sawicki, "Maximal freedom at minimum cost: linear large-scale structure in general modifications of gravity", JCAP **07** (2014) 050, doi:10.1088/1475-7516/2014/07/050, arXiv:1404.3713.

[5] P. Creminelli, M. Lewandowski, G. Tambalo, and F. Vernizzi, "Gravitational wave decay into dark energy", JCAP **12** (2018) 025, doi:10.1088/1475-7516/2018/12/025, arXiv:1809.03484; P. Creminelli, G. Tambalo, F. Vernizzi, and V. Yingcharoenrat, "Dark-energy instabilities induced by gravitational waves", JCAP **05** (2020) 002, doi:10.1088/1475-7516/2020/05/002, arXiv:1910.14035v2.

[6] W. J. Wolf, P. G. Ferreira, and C. García-García, "Cosmological constraints on Galileon dark energy with broken shift symmetry", Phys. Rev. D **113**, 023551 (2026), corrected by APS on 24 February 2026, doi:10.1103/bxvj-bsv1, arXiv:2509.17586v3.

[7] C. García-García, P. G. Ferreira, and W. J. Wolf, "The status of single scalar field dark energy", accepted in Phys. Rev. D (2026), doi:10.1103/jkcl-g4cq, arXiv:2607.07777v3.

[8] S. Tsujikawa, "Crossing the phantom divide in scalar-tensor and vector-tensor theories", Phys. Rev. D **113**, L041301 (2026), doi:10.1103/y858-4swl, arXiv:2508.17231v2.

[9] W. Handley, "`anesthetic`: nested sampling visualisation", J. Open Source Softw. **4**(37), 1414 (2019), doi:10.21105/joss.01414, arXiv:1905.04768. Software version 2.10.2, commit `b6076caf`.

[10] M. Cataneo and K. Koyama, "Non-parametric exploration of minimally coupled gravity with phantom crossing", Phys. Rev. D **113**, 122006 (2026), doi:10.1103/ckns-5ytv, arXiv:2512.13691v2.

[11] T. Borislavov Vasilev, M. Bouhmadi-López and P. Martín-Moruno, "Dark energy with a shift-symmetric scalar field: obstacles, loophole hunting and dead ends", arXiv:2406.12576v2 (2024).

[12] E. V. Linder, "Cosmology after Phantom Crossing by Horndeski Gravity", arXiv:2512.03139v2 (2025).

[13] M. Zumalacárregui, E. Bellini, I. Sawicki, J. Lesgourgues, and P. G. Ferreira, "`hi_class`: Horndeski in the Cosmic Linear Anisotropy Solving System", JCAP **08** (2017) 019, doi:10.1088/1475-7516/2017/08/019.